ELSEVIER

1359-8368(95)00037-2

Composites Part B **27B** (1996) 531–541

1359-8368/96/$15.00

Compressive R-curve of a carbon fibre–epoxy matrix composite

N. A. Fleck, M. P. F. Sutcliffe, S. Sivashanker and X. J. Xin
Cambridge University Engineering Department, Trumpington Street, Cambridge, CB2 1PZ, UK
(Received 17 August 1995; accepted 10 October 1995)

The development of microbuckling from a sharp notch under remote compressive loading is investigated for a unidirectional carbon-fibre/epoxy composite. Experimental measurements of the overall kink-band width confirm that a growing microbuckle propagates in a crack-like manner rather than like a dislocation. A large-scale bridging model with a crack tip toughness and a constant bridging stress is successful in correlating the length and width of a growing microbuckle with the remote stress. This R-curve behaviour is modelled using a finite element analysis. The effect of matrix yield strain on the R-curve is significant, while the influence of the matrix strain-hardening rate and initial fibre waviness is slight. Prediction of the initiation of microbuckling is found to be in good agreement with experimental data for a carbon-fibre/epoxy composite. Copyright © 1996 Elsevier Science Limited

(Keywords: compression; R-curve; toughness; fracture mechanics; microbuckling)

INTRODUCTION

Long-fibre/polymer matrix composites, such as carbon fibres in an epoxy matrix, possess excellent tensile properties resulting from the high tensile strength of the fibres. However, they fail in compression by plastic microbuckling at stresses of only about 60% of their tensile strength[1,2]. Structural components made from long-fibre composites typically contain fastener holes and cut-outs; they may also suffer service damage, for example in the form of holes, fibre fractures and delaminations. These imperfections reduce the compressive strength by inducing stress concentrations and by promoting the initiation and propagation of microbuckles.

When a sharp notch is loaded in compression*, the relationship between the applied stress intensity factor and the microbuckle length gives an R-curve characterising the resistance of the microbuckle to growth. This R-curve behaviour can be modelled using a compressive tip toughness K_c and a constant bridging stress behind the microbuckle tip σ_b[3].

Sutcliffe and Fleck[4,5] investigated the effect of the specimen size relative to the bridging length scale $r_p = K_c^2/\sigma_b^2$ on the transition between small-scale and large-scale bridging of notched specimens. They concluded that, if the bridging length scale r_p is small compared with the specimen dimensions, the R-curve behaviour does not depend on the geometry of the specimen. The specimen fails when the stress intensity at the tip of a sharp notch equals a critical compressive stress intensity factor, which will have contributions from the tip toughness and from the bridging stresses behind the tip. This compressive fracture toughness has been measured for a wide range of lay-ups of T800/924C carbon/epoxy material with centre-cracked specimens[2]. The measured value of the fracture toughness is found to be independent of initial notch length, in support of the concept of a compressive fracture toughness. When r_p is not small compared with either the initial notch length or the unnotched ligament then large-scale bridging theory must be used. In this regime it is necessary to include details of the crack bridging law in a cohesive zone calculation to predict the failure load accurately; furthermore, the R-curve is no longer a material property but also depends on the geometry of the component.

Compressive failure from a hole in a composite laminate has been modelled with varying degrees of sophistication, including the maximum local stress criterion[6], the net section stress criterion, the average stress failure criterion[7], the point stress failure criterion[8], the Whitney and Nuismer model[9] and more recently the Soutis *et al.* model[10]. The latter model[10] is based on the

* We consider here notches which, although sharp enough to generate a large stress concentration factor at the tip, nevertheless have a sufficient clearance across the notch to prevent crack closure under compressive loading

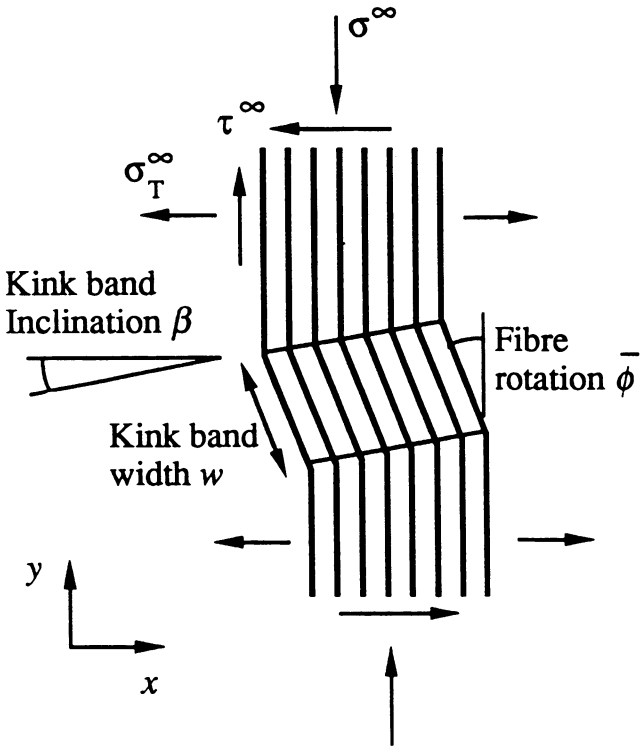

Figure 1 Infinite kink band in a unidirectional composite. Fibres within the band have an initial misalignment angle $\bar{\phi}$

notion of a cohesive zone in which damage around an open hole is represented by a line-crack loaded with a normal compressive traction. This engineering model takes as its input a compressive tip toughness and the unnotched strength of the laminate. From the design and manufacturing points of view, it is desirable to predict the unnotched strength and the compressive toughness from the mechanical properties of the basic material constituents: the fibres, matrix and the lay-up geometry.

It is now well established that the unnotched compressive strength σ_c is governed by *imperfection-sensitive plastic microbuckling* and that the imperfection exists in the form of fibre misalignment[11–14]. Slaughter *et al.*[15] considered microbuckling from an infinite band of uniform fibre misalignment $\bar{\phi}$ as shown in *Figure 1*; the unidirectional composite is subjected to a remote axial stress σ^∞ parallel to the fibre direction, an in-plane transverse stress σ_T^∞ and an in-plane longitudinal shear stress τ^∞. The infinite band is inclined with respect to the fibre axes such that the normal to the band is rotated by an angle β with respect to the nominal fibre direction, as shown in *Figure 1*. The transverse direction may be either the through-thickness direction of the panel, in which case *Figure 1* represents an 'out-of-plane' microbuckle, or it may lie in the plane of the panel; *Figure 1* then represents an 'in-plane' microbuckle. For the case where the composite displays a rigid–perfectly plastic in-plane response, the compressive strength is given by

$$\sigma_c \approx \frac{\tau_y - \tau^\infty - \sigma_T^\infty \tan\beta}{\bar{\phi}} \qquad (1)$$

where τ_y is the shear yield strength of the composite[15].

By using the above kinking theory, the unnotched strength of a unidirectional lay-up may be predicted in terms of the shear properties of the composite, the fibre misalignment angle and the remote multi-axial stress state. On the other hand, a theoretical study of the prediction of the compressive fracture toughness and hence the R-curve behaviour has been lacking.

In this paper we present experimental observations of microbuckle initiation and growth to support the use of a crack model for microbuckle growth. The R-curve behaviour of a carbon-fibre/epoxy composite is measured and used to estimate tip toughness and bridging stress. Overlap displacements across the microbuckle faces are compared with the results of a large-scale bridging model. Having confirmed the validity of the crack model for failure at sharp notches, a finite element analysis is used to analyse this behaviour. The sensitivity of the R-curve to the matrix shear strength is determined and a comparison is made with the experimental observations.

Experimental measurements of initiation and R-curve behaviour

The investigation of kink-band growth in fibrous polymer composites can be difficult, since unstable propagation often occurs as soon as kinking is initiated. Notched unidirectional T800/924C carbon-fibre/epoxy composites typically split at the notch ends when loaded along the fibre direction. Sutcliffe and Fleck[3] succeeded in encouraging miocrobuckle growth from a sharp centre notch by having an additional vertical notch, cut in the fibre direction along the mid-plane of a centre notch.

In the present investigation we use two techniques to overcome this problem. For an investigation of the initiation of microbuckling we use the above technique to inhibit splitting at the microbuckle tip. To investigate the R-curve behaviour, we first nucleate a microbuckle and then monitor its propagation under compressive loading. With this technique we succeed in obtaining stable microbuckle growth in a consistent, repeatable manner for microbuckle lengths limited only by the ligament length of the specimen (35 mm for the geometry employed).

Experimental techniques

Specimen design. The material system consists of Toray T800 carbon fibres in Ciba Geigy 924C epoxy matrix. All specimens were of unidirectional lay-up and were nominally 3 mm thick and 50 mm wide. Aluminium end tabs were bonded to the specimen ends using a hot cure epoxy adhesive to enable a smooth transfer of load.

For the initiation tests a centre notch of length 25 mm was cut into the specimens and sharpened using a razor blade. In one case the faces of the specimen at the tip of the notch were restrained against out-of-plane movements using small square plates. The average clamping pressure was about 50 MPa. These specimens will be

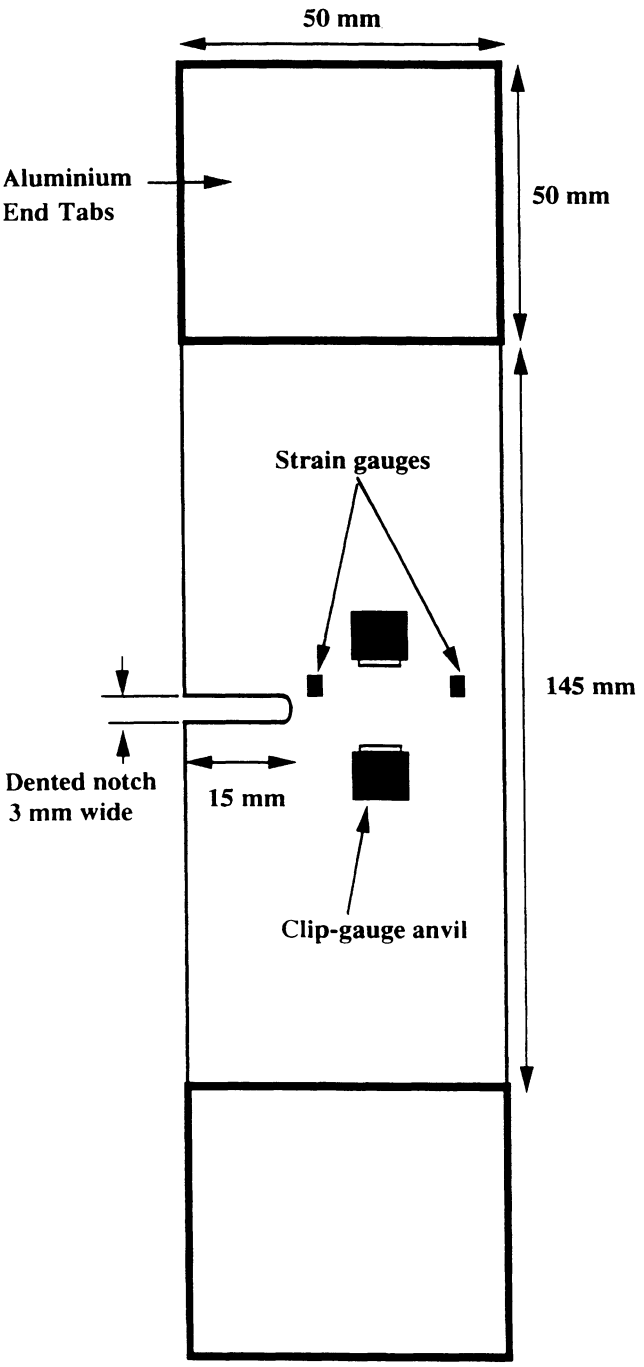

Figure 2 Specimen geometry. Gauge length of clip gauge is 10 mm

referred to as 'clamped specimens'. In general, however, the free surfaces at the notch tip were unrestrained against out-of-plane displacements.

For the R-curve tests an edge notch, 15 mm long and 3 mm wide, was machined into the specimen. A roller bearing of diameter 2 mm was then used to indent the notch root while loading the specimens in three-point bending. This indentation nucleated a microbuckle at the notch root with a length of about 2 mm. The front face of the test specimen was scribed with lines along the fibre direction using a diamond tool fitted to an Omicron co-ordinate measuring machine. The line spacing was at 2 mm intervals commencing from the edge of the notch. These lines were then filled with white engraver's wax. This enabled the position of the microbuckle tip to be deduced at any stage during high magnification videography, since only a portion of the specimen around the microbuckle tip could be viewed at any instant. The specimen geometry for the R-curve tests is shown in *Figure 2*.

Mechanical testing and examination. The specimen was held in wedge grips and loaded in compression using a screw-driven test machine in displacement control. Anti-buckling guides lubricated with PTFE spray prevented Euler macrobuckling of the specimen. Special attention was given to specimen alignment between the lower and upper wedge grips.

For the R-curve tests the region in the vicinity of the notch root was projected on to a TV screen and video recorder using a high-magnification video camera. This set-up enables one to follow the damage events easily, and gives a permanent record of the test. The initial loading rate was 0.01 mm s^{-1}. Upon the first sign of damage propagation the loading rate was reduced to 0.001 mm s^{-1} to slow down the stable microbuckle propagation.

Observations of microbuckle initiation

Figures 3(a) and *(b)* show optical micrographs of the

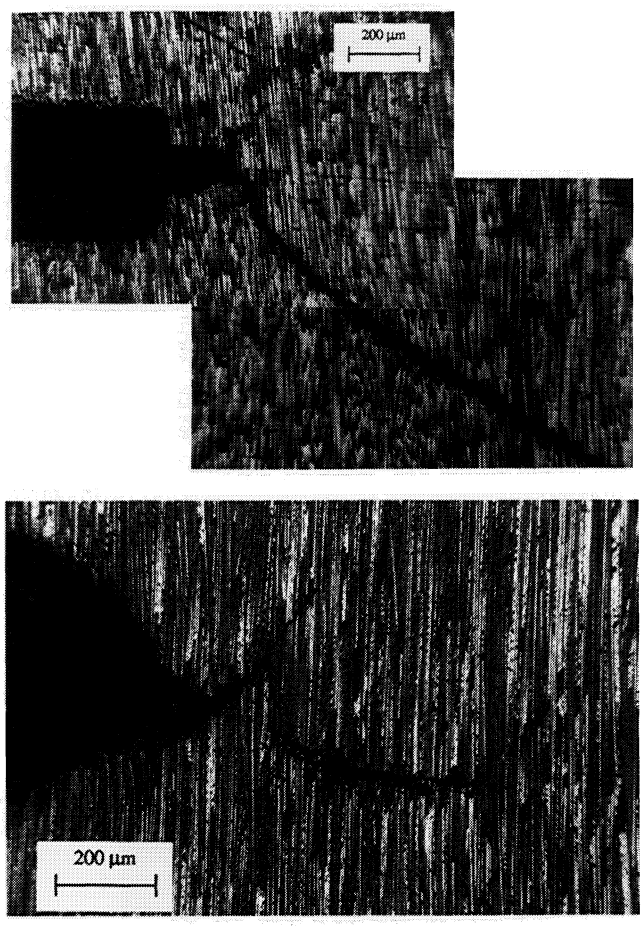

Figure 3 Optical micrograph of the notch tip at initiation, (a) clamped to restrain out-of-plane movements, (b) unclamped

tips of the clamped and unclamped specimens, respectively. Both specimens show two short in-plane microbuckles initiating from the notch tip, but only one subsequently growing away from the notch. For the clamped specimen [*Figure 3(a)*] the long microbuckle continues to grow as an in-plane microbuckle; the propagation direction changes as the microbuckle grows. Near the notch tip, the normal to the microbuckle lies at an angle of about 45° to the fibre direction; away from the notch tip this angle is about 25°. For the unclamped specimen [*Figure 3(b)*] the longer propagating microbuckle has switched from buckling in-plane to out-of-plane microbuckling, with the transverse direction of propagation of the microbuckle at 90° to the fibre direction.

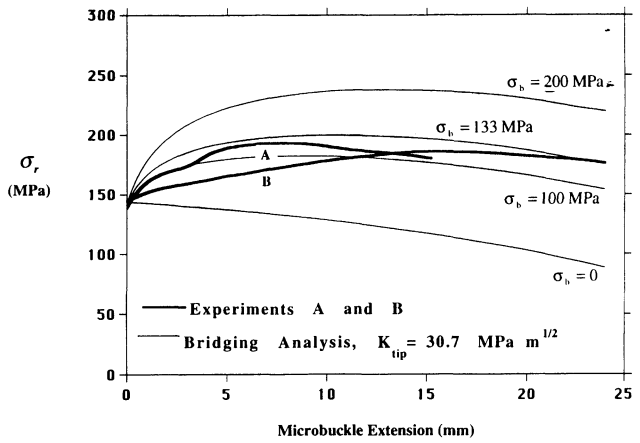

Figure 5 Comparison of measured collapse response with predictions from the large-scale crack bridging model

R-curve behaviour

In this series of tests we are concerned with the R-curve behaviour of the microbuckle after initiation. Two types of experiment were conducted with this test set-up: experiment A and experiment B as follows.

Experiment A. In experiment A, the specimen was unloaded and the test terminated when the kink band had propagated part-way through the ligament. This specimen was subsequently examined in the scanning electron microscope.

Experiment B. In experiment B, the microbuckle was allowed to propagate across the entire width of the ligament. Foil strain gauges were placed on the rear face 1.5 mm above the expected trajectory of the microbuckle. One strain gauge was placed 4 mm from the notch tip and a second gauge was placed 24 mm from the notch tip. A clip gauge of gauge length 10 mm was also located on the rear face, 14 mm from the notch tip (see *Figure 2*). The strain, load and clip-gauge readings were recorded every half second using a computerised data logger.

Out-of-plane microbuckling. Visual observation of the specimens revealed that out-of-plane microbuckling occurred in both experiments A and B. *Figure 4* shows a magnified view of the kink-band which has propagated mid-way across the specimen ligament in experiment A. The arrested microbuckle extends 16 mm from the notch root. The material is microbuckling out-of-plane with the normal to the kink band inclined at an angle of about 25° to the fibre direction. The microbuckle behaves as a mode I crack, such that the material above the microbuckle band slides over that below. The extent of this sliding increases with increasing distance from the microbuckle tip. At the tip of the microbuckle there is one kink band of broken fibres, while behind the tip a second band of broken fibres has formed.

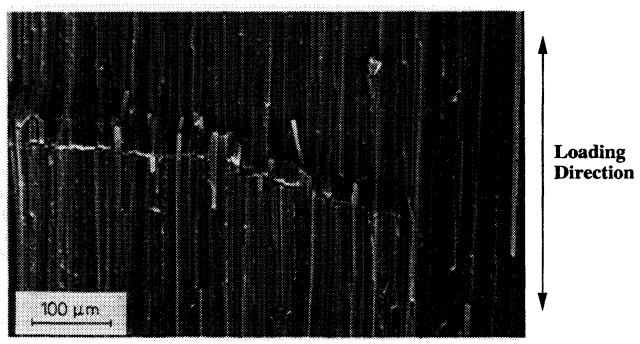

Figure 4 Tip of growing microbuckle after unloading, showing progressive development of multiple kinking

Microbuckle growth versus *applied stress.* Microbuckle extension is shown as a function of remote stress σ_r in *Figure 5*, for both experiments A and B. The initial part of this R-curve will be independent of the specimen geometry, but when the microbuckle is no longer short compared with the notch and ligament lengths (15 and 35 mm, respectively), then the behaviour will be a function of both the geometry and the material. We note that microbuckle propagation begins at $\sigma_r \approx 140$ MPa, followed by an increase in σ_r to a plateau value of about 180 MPa.

Measurements of local bridging stresses. The bridging stresses across the growing microbuckle were measured using strain gauges in experiment B. The results are shown as a function of the microbuckle tip location in *Figure 6*. We note that the axial stress measured by each strain gauge attains a maximum when the microbuckle tip lies adjacent to the gauge. For the strain gauge placed 4 mm from the notch root, the bridging stress asymptotes to a constant value of about 100–130 MPa in magnitude. These values are in good agreement with measurements made by Sutcliffe and Fleck[3] who considered specimens containing a microbuckle across the full ligament: these previous tests measured the rubble strength to be in the range of 138–146 MPa.

Kink-band width measurements. After completion of experiment A, the side faces of the specimen were examined in the scanning electron microscope. Multiple kink

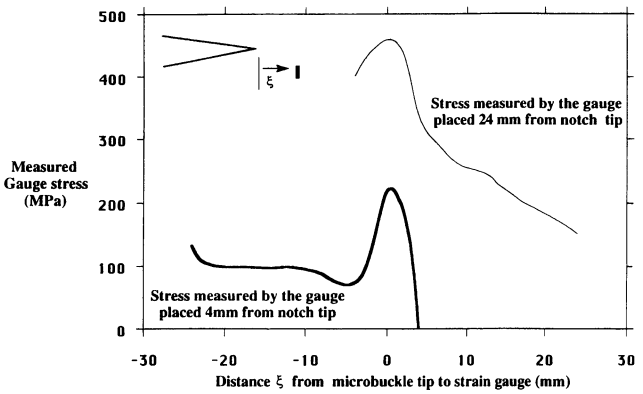

Figure 6 Strain-gauge stress as a function of distance from the microbuckle tip

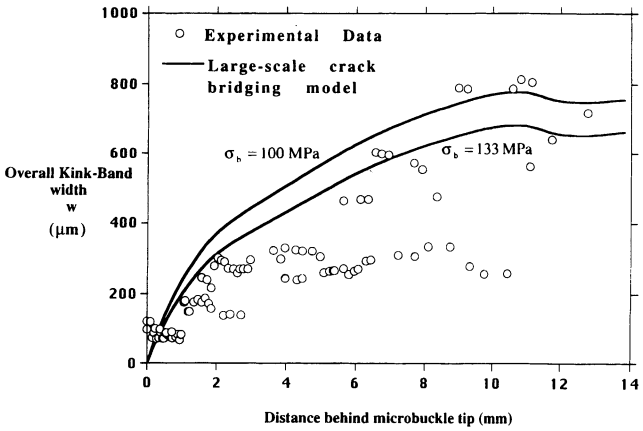

Figure 7 Comparison of measured overall microbuckle width with predictions from large-scale crack bridging model

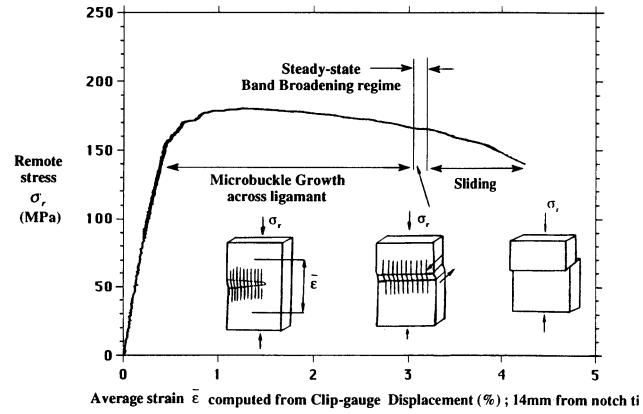

Figure 8 Collapse response of specimen in experiment B

bands were observed, as illustrated in *Figure 3*. Such multiple kink-band formation has also been reported previously by Sutcliffe and Fleck[3]. The width of the *overall* kink band increases from about 70 μm at the microbuckle tip to about 800 μm at the notch root. The variation in microbuckle width along the length of the microbuckle is plotted in *Figure 7*. The number of individual kink bands increases from a single band at the microbuckle tip to about six bands at the notch root, while the width of the *individual* kink bands is constant at about 100 μm (i.e. 20 fibre diameters). This measured width of individual kink bands supports the predicted width of 15–20 fibre diameters by Fleck *et al.*[14].

Band-broadening. It is clear from *Figures 4* and *7* that a microbuckle advances in a crack-like manner, with broadening of the microbuckle behind its tip. The bridging stress across the microbuckle flanks settles down to a constant value (see the gauge stress measured at 4 mm from the notch root in *Figure 6*). After the microbuckle has grown across the specimen ligament in experiment B, the microbuckle continues to broaden in the fibre direction under a constant applied stress (see *Figure 8*). Steady-state band broadening is superseded by the sliding-off of the two halves of the specimen along one of the kink-band fracture planes. This is sketched in *Figure 8*.

The phenomenon of steady-state band broadening has been reported previously by Moran *et al.*[16] for an IM7 carbon-fibre/PEEK composite. The IM7 fibres have sufficient strength to remain intact during microbuckling, and so multiple kink bands were not observed by Moran *et al.*[16]. In other respects, however, our findings are in agreement with theirs. The phenomenon consists of steady-state buckle propagation, whereby unbuckled fibres are convected to a buckled state under constant remote stress.

The observations described above show that kink-bands propagate as a crack and not as a dislocation. If microbuckle propagation were akin to dislocation motion, we would expect to observe constant kink-band widths and a fixed value of shear displacement across the microbuckle. A dislocation mode of the microbuckle propagation mode has been suggested in several past studies on kink-band propagation[17,18].

Comparison with a large-scale crack bridging model

In this section we describe the results of a large-scale bridging analysis used to model the experimentally observed collapse response. A large-scale crack bridging model is employed on the basis that a microbuckle propagates in a crack-like manner. Accordingly, we treat the out-of-plane microbuckle as a bridged mode I crack in compression. The crack is ascribed a tip toughness G_{IC} and a constant normal bridging stress along its flanks. The constant crack bridging stress is associated with the phenomenon of steady-state band broadening. We take this normal bridging stress to be a constant and to possess the value measured experimentally of between 100 MPa and 133 MPa. The analysis considers the superposition of the stresses due to the remote applied load and due to the bridging stress behind the microbuckle tip. Calculations given by Wu and Carlsson[19] are used to calculate the stress intensity factor at the tip of the microbuckle. The applied remote stress is then found as a function of the microbuckle length by using the condition that this tip stress intensity factor equals the material critical stress intensity factor. The

corresponding overlap displacements can be found using the results of Wu and Carlsson[19]. Details of the analysis are given in ref. 20.

Although the specimen used in the current study is a single edge-notch specimen, we model it by a centre-notch configuration. Under prescribed end loads, single edge-notch specimens rotate due to their asymmetrical geometry. In practice the clamping action of the wedge grips allows little rotation of the specimen ends. This resistance to end-rotation results in an end-moment which has to be taken into account in any full analysis of the single edge-notch specimens. We avoid the complication of this end-moment in our computation by treating the specimen geometry as being equivalent to one half of a centre-notch geometry. Sutcliffe and Fleck[5] have verified experimentally that the effect of clamping a single edge-notch specimen is to make it behave like a half centre-notch specimen under uniform axial stress.

The measured microbuckle-initiation stress of 140 MPa in both experiments A and B is used to deduce a crack tip fracture toughness of $K_C = 30.7\,\text{MPa}\,\text{m}^{1/2}$. The tip toughness G_C, which equals $17.3\,\text{kJ}\,\text{m}^{-2}$, is found from the fracture toughness K_C by the relation $K_c^2 = E'G_c$, where the equivalent elastic modulus E' is defined by

$$\frac{1}{E'} = \left(\frac{1}{2E_{xx}E_{yy}}\right)^{1/2}\left[\left(\frac{E_{yy}}{E_{xx}}\right)^{1/2} - \nu_{yx} + \frac{E_{yy}}{2G}\right]^{1/2} \qquad (2)$$

and equals 54.8 GPa for a T800/924C unidirectional laminate. Here, the x-axis is aligned with the fibre direction, and the y-axis is along the in-plane orthogonal direction.

Predictions of the microbuckle length as a function of applied stress are given in *Figure 5*, for a range of assumed values for the crack bridging stress σ_b. Recall that it was found experimentally that the local bridging stress σ_b ranges from 100 MPa to 133 MPa for the T800/924C unidirectional laminates (*Figure 6*). The measured collapse response (applied stress *versus* microbuckle length) in experiment A is bounded by the predictions for $\sigma_b = 100$ MPa and $\sigma_b = 133$ MPa (see *Figure 5*). Agreement is less satisfactory for experiment B: although test parameters were nominally identical, specimen B was somewhat weaker than specimen A during the early stages of microbuckle propagation and the measured collapse response is below both predictions for $\sigma_b = 100$ MPa and $\sigma_b = 133$ MPa. Note that the predicted response is sensitive to the precise value of σ_b: the predicted collapse curve for $\sigma_b = 0$ lies much lower than the measured response. In contrast, an assumed value of $\sigma_b = 200$ MPa gives a much stronger response than that observed experimentally.

To give further credence to the large-scale crack bridging model we compare in *Figure 7* the predicted microbuckle width along the microbuckle length for the centre-notch configuration with the measured microbuckle width. The predicted values assume that $K_C = 30.7\,\text{MPa}\,\text{m}^{1/2}$ and σ_b lies in the range 100–133 MPa. We deduce the microbuckle width w from the overlap displacement δ, by considering the kinematics of the displacements across the microbuckle faces. We assume that the fibres in the out-of-plane microbuckle have rotated by twice the measured inclination angle of 25°; δ is the component of the out-of-plane displacements resolved in the in-plane direction. It is clear from *Figure 7* that the crack theory adequately predicts the observed trend of increasing microbuckle width with distance behind the microbuckle tip. The good agreement between the large-scale crack bridging model predictions and experimental observations support our claim that a growing microbuckle is a crack-like feature. This conclusion was also reached in earlier work by Sutcliffe and Fleck[3].

THEORETICAL CALCULATIONS OF R-CURVES

Experimental observations described in the previous section have confirmed that a propagating microbuckle can be modelled as a crack with a tip toughness and a bridging stress. In this section we describe finite element results which calculate the tip toughness from the properties of the matrix and fibres, and compare the predictions with the experiments described above.

Finite element formulation

Consider a composite panel containing a sharp edge notch of length a under remote compressive loading. When the region of non-linearity at the tip of the crack is small compared to the crack length, the non-linear region is embedded within the crack tip elastic K-field and the condition of 'small-scale yielding' is met. Then, the stress field in the vicinity of the crack tip can be determined using a boundary layer formulation: a domain containing a crack is loaded on its outer boundary by a compressive K-field of mode I type. In the present study we make use of the commercial finite element code ABAQUS[25] to examine the development of microbuckling from the tip of the traction-free crack in a unidirectional composite under a compressive mode I K-field.

Finite element mesh. A sketch of the small-scale yielding problem is shown in *Figure 9(a)*. The initial notch is aligned with the x direction and the fibres are parallel to the y direction. A full mesh is employed in order to allow for the existence of non-symmetric crack tip buckling modes. The outer boundary of the mesh is subjected to the displacement field associated with a compressive mode I stress intensity factor in an orthotropic elastic solid, as given by Paris and Sih[21]. Two distinct regions of mesh are distinguished in *Figure 9(a)*: an *outer mesh* and an *inner mesh* [detailed in *Figure 9(b)*]. The inner mesh consists of alternating layers of fibres of thickness d, and of matrix of thickness t. The relative magnitudes of d and t are chosen to achieve a fibre volume fraction $c = d/(d+t) = 2/3$. Since the fibres carry significant bending stresses during microbuckling they are represented by 8-noded quadratic-interpolation elements; the matrix

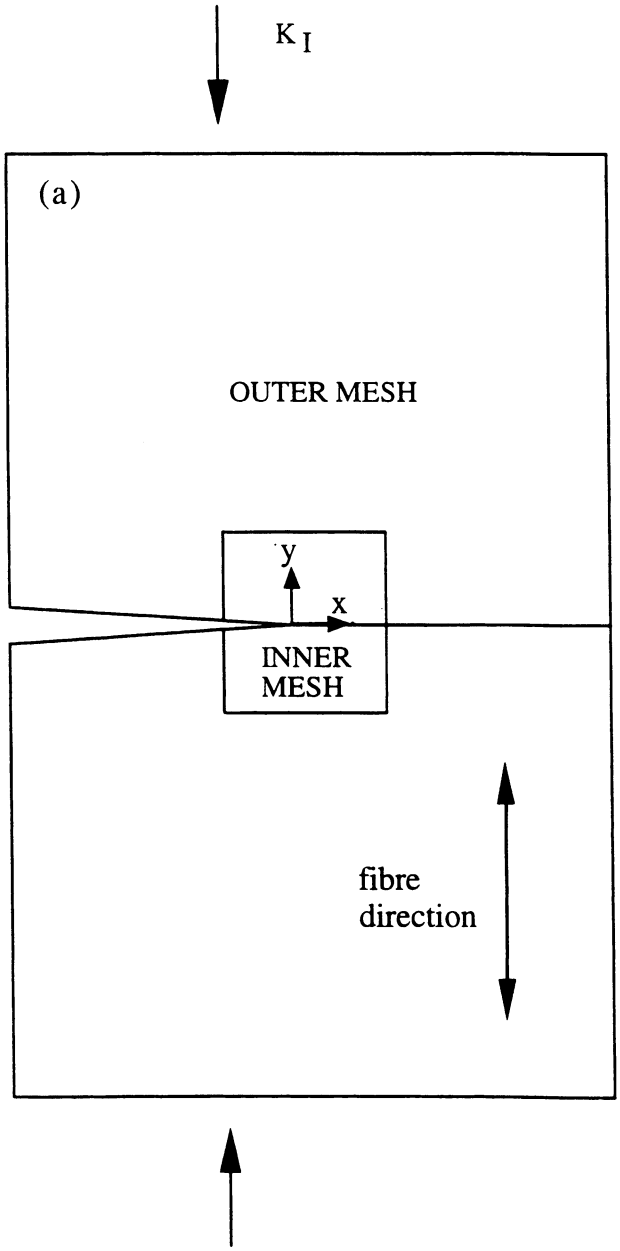

Figure 9 (a) Sketch of a unidirectional composite with a semi-infinite crack under a remote mode I stress intensity factor K_I

undergoes predominantly plastic shear deformation and is represented by 4-noded linear-interpolation elements. For the inner mesh shown schematically in *Figure 9(b)* there are 25 fibres ahead of the crack tip, and 6 fibres behind the crack tip; the inner zone of the mesh is of height $36d$. The tip of the crack is located at the boundary between a matrix layer and a fibre layer, with a fibre immediately ahead of the crack tip and the adjacent matrix layer immediately behind the crack tip. Unless otherwise stated, all fibres are straight in the undeformed configuration.

Limitations of computer memory and computation time preclude modelling of the outer mesh by alternating layers of fibre and matrix elements. Instead, the outer mesh is modelled by a combination of:

(i) 4-noded linear-interpolation elements with elastic–plastic properties representative of the composite;

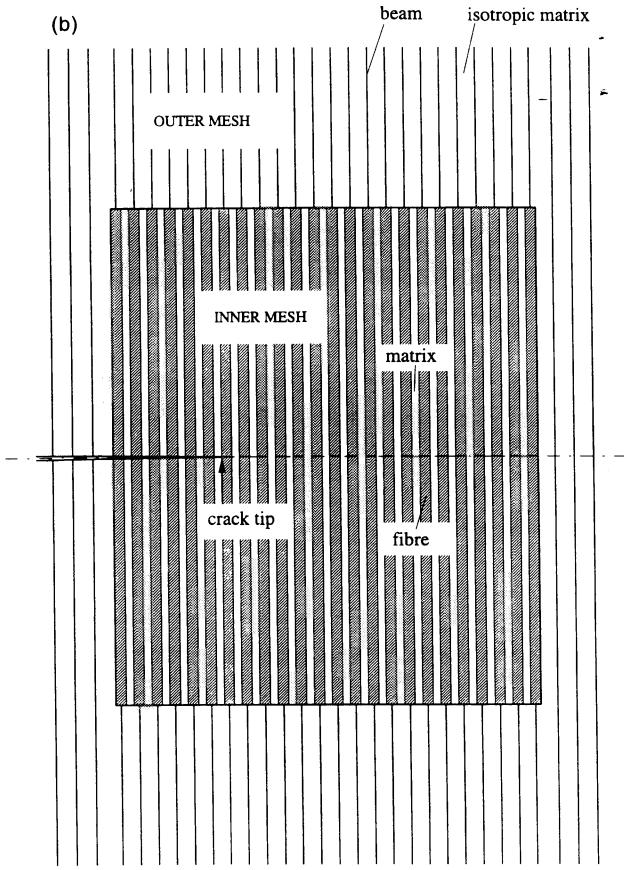

Figure 9 (b) Details of mesh near crack tip. The inner mesh consists of alternating fibre and matrix elements, while the outer mesh consists of matrix and beam elements

(ii) embedded beam elements to mimic the finite fibre bending resistance and to provide the main contribution to the longitudinal stiffness E_{yy} of the composite.

The full mesh has 6676 elements and the ratio of the inner mesh area to the total mesh area is 3.6×10^{-4}. Material properties for the inner and outer meshes are given below. Small-scale yielding conditions are maintained by ensuring that the plastic zone size is much less than the overall mesh size.

Material properties of the composite. The composite is treated as a deformation theory elastic–plastic solid with a Ramberg–Osgood hardening behaviour. When the composite is loaded by an in-plane shear stress τ parallel to the fibre direction, the shear strain γ is given by

$$\frac{\gamma}{\gamma_y} = \frac{\tau}{\tau_y} + \alpha_c \left(\frac{\tau}{\tau_y}\right)^n \tag{3}$$

where τ_y is the shear yield strength, γ_y is the shear yield strain and n is the strain-hardening exponent. The shear modulus G equals τ_y/γ_y and α_c is taken as 3/7. The Ramberg–Osgood parameters used in our calculations are summarised in *Table 1*. For the majority of the calculations we select the material properties to represent those of unidirectional Toray T800 carbon fibres in a

Table 1 Materials constants used in the calculations

	Composite	Inner mesh: fibres	Inner mesh: matrix	Outer mesh: 4-noded elements
E_{xx} (GPa)	9.25	240	6.4	18
E_{yy} (GPa)	162	Isotropic	Isotropic	Isotropic
G (GPa)	6.8	91	2.3	6.7
ν_{xy}	0.0195	0.32	0.40	0.34
σ_y ($= \sqrt{3}\tau_y$) (MPa)	10.8–1080	—	10.8–1080	10.8–1080
α	3/7	—	3/7	3/7
n	3.5–100	—	3.5–100	3.5–100

Unless otherwise stated, $n = 3.5$ and $\sigma_y = 108$ MPa ($\gamma_y = 9.2 \times 10^{-3}$), when material properties are typical of unidirectional T800/924C carbon-fibre/epoxy material

Ciba-Geigy 924C epoxy matrix. This material has been intensively examined within the authors' laboratory[22] and its Ramberg–Osgood parameters have been measured by Jelf and Fleck[23]. The fibres are taken to be isotropic and linear elastic, with a Young's modulus of $E_f = 240$ GPa and a Poisson's ratio of $\nu_f = 0.32$. These values are typical of Toray T800 carbon fibres, which have a fibre diameter $d = 5\,\mu$m.

The properties of the elastic–plastic and beam elements in the outer mesh are chosen to give similar in-plane effective properties for the composite as for the inner mesh region. Further details of the material characterisation and the finite element formulation are given in ref. 24.

Finite element predictions of the R-curve

Finite element results are now presented for the R-curve behaviour for a microbuckle growing from a sharp notch. Firstly, results are given for the evolution of the deformation fields as a function of remote K_I. The sensitivity of the microbuckling response to composite material yield strength and strain-hardening exponent is then examined.

Development of microbuckling from the notch tip. Details of the microbuckle development are presented in this section, with material properties chosen to represent a unidirectional T800/924C carbon-fibre/epoxy composite. The deformed mesh is shown in *Figure 10* at three levels of applied K_I, labelled A, B and C. Under increasing compressive K_I, the fibres near the crack tip rotate and the matrix suffers combined shear and transverse straining. At low levels of applied load (such as state A, $K_I/G\sqrt{d} = 1.8$) the deformation state is nearly symmetric about the crack plane. The crack profile is shown by overlapping of traction-free crack flanks behind the tip. At a higher load (state B, $K_I/G\sqrt{d} = 2.6$) a pronounced buckle develops at the crack tip; the buckle is asymmetric with respect to the crack plane. Under a further increase in K_I, the buckle spreads in the transverse x direction and can be considered to be composed of two microbuckles inclined at $\pm 20°$ with respect to the transverse x direction, as shown by state C in *Figure 10*. Nucleation of the microbuckle involves large tensile transverse strains in the matrix layer surrounding the crack tip. The current analysis includes neither failure of the matrix nor of the fibres: if transverse failure of the matrix were to be incorporated into the analysis then a split would develop at the crack tip, and blunt the stress concentrating effects of the crack tip. In practical carbon-fibre/epoxy laminates, the off-axis plies lie adjacent to the 0° plies and prevent split formation under compressive loading[2]. Since the purpose of the work is to explore microbuckle development in the 0° plies and so provide insight into the compressive response of practical multi-directional laminates, split development was not investigated further.

To deduce the relationship between the extent of microbuckling and the level of compressive K_I we need to define the boundary of the microbuckle zone. Microbuckling results in a drop in the load-carrying capacity of the fibres. The microbuckle length is determined by comparing the mean axial stress in the composite directly ahead of the crack tip with the axial stress associated with the compressive, mode I, elastic K-field*. While at the lowest loads the stress distribution is very nearly that of the elastic solution, as the load is increased the stresses fall below the elastic solution for a considerable region ahead of the crack tip. We arbitrarily define the extent of the microbuckle as the region where the axial stress lies more than 10 percent below the elastic stresses.

The projected length of the buckle l along the transverse x direction is plotted as a function of K_I in *Figure 11(a)*: we refer to this plot as the compressive R-curve for the composite. States A–C illustrated in *Figure 10* are marked on the corresponding curve in *Figure 11(a)* with $n = 3.5$. A local maximum in the R-curve is observed at $K_I/G\sqrt{d} = 2.6$ [corresponding to state B of *Figure 10(b)*]. In order to capture this snap-back phenomenon under prescribed K-loading, the Riks' algorithm is used within the ABAQUS program[25].

Effects of material properties on the R-curve. Infinite band calculations for the initiation of microbuckling[13,17] suggest that the unnotched compressive strength increases linearly with the shear strength of the matrix and is inversely proportional to the degree of fibre misalignment $\bar{\phi}$, as given by equation (1).

*To facilitate the method, the mean axial stress distribution in the composite was found by multiplying the axial strain in the beam elements and at the centre of fibres directly ahead of the crack by the axial modulus of the composite

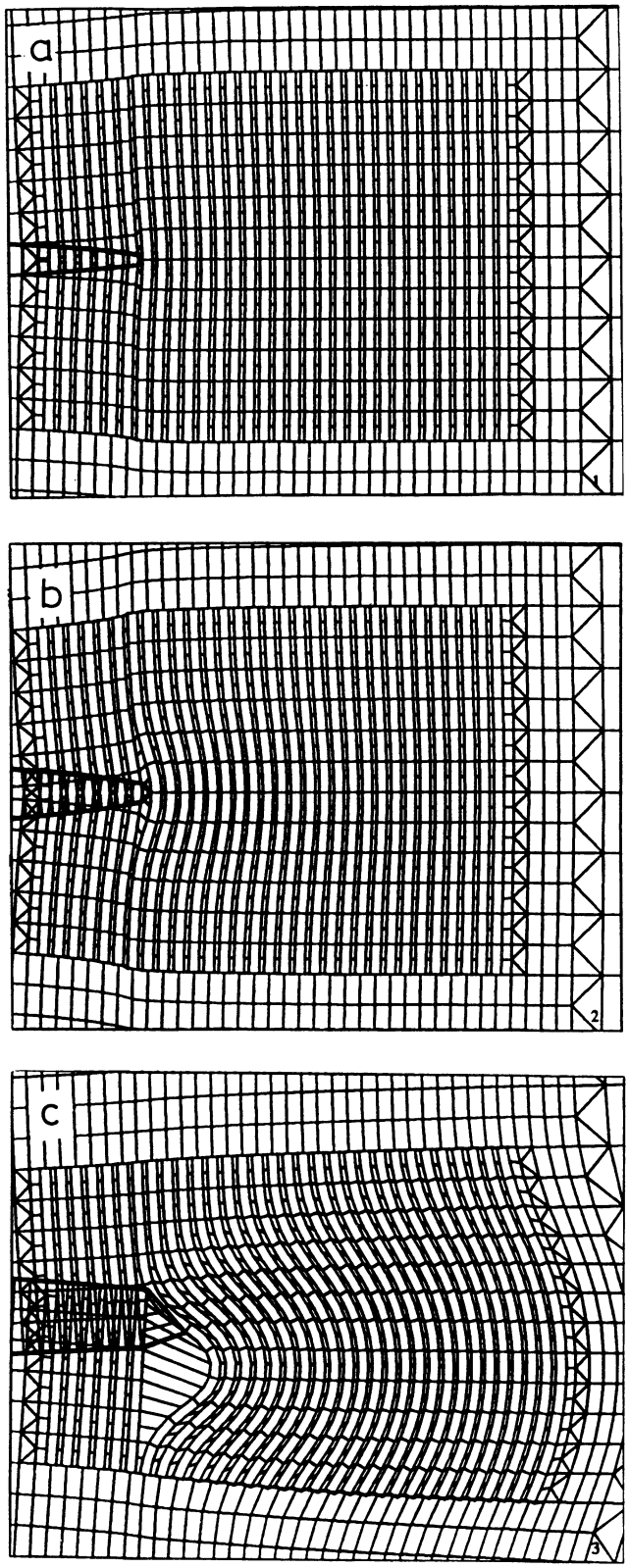

Figure 10 Deformed mesh at three stages of compressive loading. No amplification of deformation is displayed. States A–C are marked on *Figure 11(a)*

Budiansky and Fleck[13] demonstrated that the infinite band compressive strength is relatively insensitive to the strain-hardening exponent n. In this section we explore whether these infinite band findings also hold for microbuckle initiation from a sharp notch.

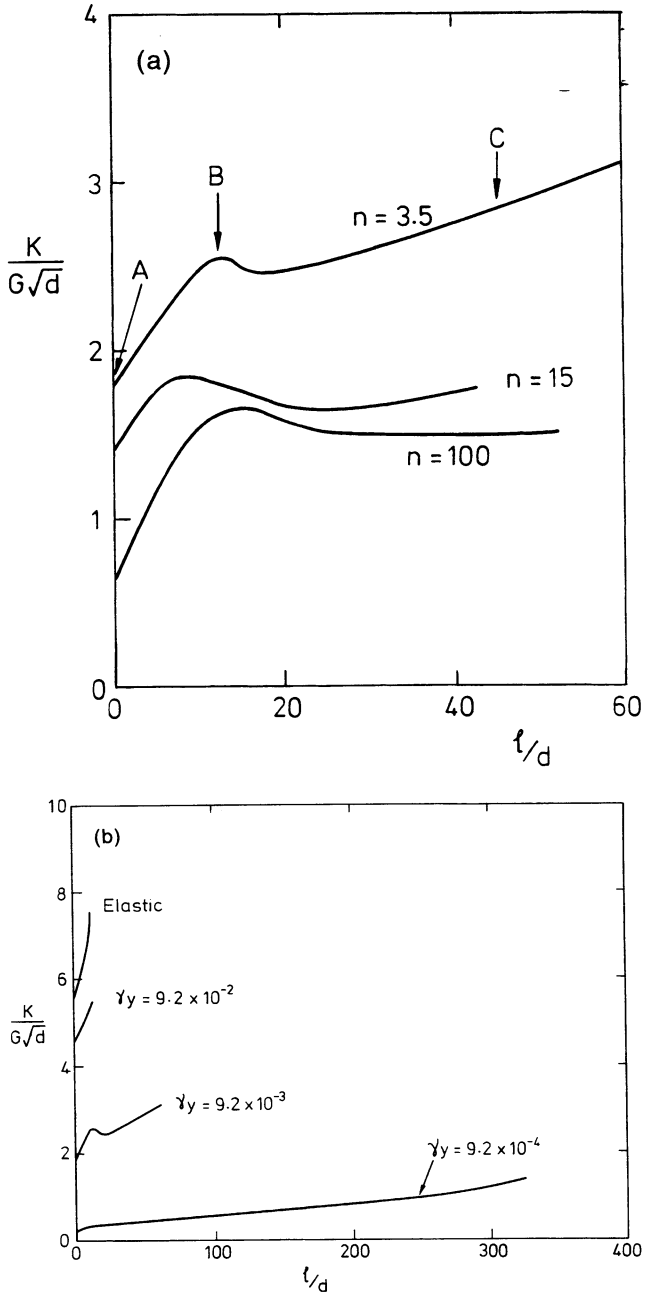

Figure 11 (a) $K_I/G\sqrt{d}$ *versus* projected microbuckle length l for a range of values of Ramberg–Osgood exponent n; $\gamma_y = 9.2 \times 10^{-3}$. (b) $K_I/G\sqrt{d}$ *versus* projected microbuckle length l for a range of values of shear yield strain γ_y; $n = 3.5$

The effects of the strain-hardening exponent n and the shear yield strength τ_y on the R-curve are shown in *Figure 11(a)* and *(b)*, respectively. The strain-hardening exponent has a moderate influence on the R-curve: when n is increased from 3.5 to 100, $K_I/G\sqrt{d}$ is reduced by a factor of about two. In *Figure 11(b)* values for the shear yield strength τ_y are presented in non-dimensional form by normalising with respect to the in-plane shear modulus G to give the shear yield strain $\gamma_y \equiv \tau_y/G$. *Figure 11(b)* also includes results for an elastic matrix. We note that the magnitude of γ_y has a significant influence on the R-curve.

Discussion. In our finite element study we have neglected the effect of fibre fracture on the microbuckling collapse. Moran *et al.*[16] have recently found that fibre fracture does not accompany microbuckle growth in IM8 carbon fibres/PEEK matrix composites. Experimental observations in the authors' laboratory of a number of carbon-fibre composites confirm these findings and show that the observed R-curve is relatively insensitive to the occurrence of fibre fracture. We surmise that the above finite element calculations of the early stages of microbuckle initiation will remain accurate when the first few fibres near the crack tip do suffer fracture during microbuckling.

It is commonly observed during microbuckling that fibres behind the microbuckle tip rotate by twice the band angle β and then 'lock up'. The role of lock-up of the matrix has been ignored in the current analysis and would need to be considered in more detail to be able to calculate the evolution of the microbuckle beyond the initiation phase.

Comparison with experimental measurements

Finite element calculations predict the initial growth of two microbuckles from a sharp crack. This is in good agreement with observations (*Figure 3*). The subsequent arrest of one of these microbuckles should be predicted by a stability analysis, while the transition from an in-plane microbuckle to an out-of-plane microbuckle would require a three-dimensional analysis beyond the scope of this paper.

An initiation compressive fracture toughness of $K_I = 30.7\,\text{MPa}\sqrt{\text{m}}$ is measured in a previous section for the T800/924C unidirectional laminate, corresponding to a value of $K_I/G\sqrt{d} = 2.0$. This is in good agreement with the initiation value for $K_I/G\sqrt{d}$ of 1.8 found from the finite element calculations [see *Figure 11(a)*]. The measured R-curve, however, does not rise as steeply as the predictions. For a value of $l/d = 60$ (corresponding to a microbuckle length of only 0.3 mm) the measured value of $K_I/G\sqrt{d} = 2.2$, while the prediction from the finite element calculation is 3.1. This difference reflects the considerably lower bridging stress found in the experiments of around 115 MPa as compared with the infinite band prediction of a bridging stress around 500 MPa for large overlap displacements. While the Ramberg–Osgood fit with a strain-hardening parameter of 3.5 is good for relatively low strains up to about 0.3, at the larger strains in the microbuckle band it predicts an unreasonably high shear strength. More accurate models of the constitutive model for the matrix at large strains are needed to improve these predictions, including the effect of cracking on softening of the matrix.

CONCLUSIONS

Experimental measurements of the overall kink-band width of an arrested microbuckle in unidirectional carbon-fibre/epoxy laminates have confirmed that a growing microbuckle propagates in a crack-like manner. The overall microbuckle width increases from about 70 μm at the microbuckle tip to about 800 μm near the notch root. During propagation, the microbuckle broadens by the formation of multiple kink bands. The preferred mode of microbuckle propagation in panels with thickness-to-width ratios much less than unity is by out-of-plane microbuckling. Out-of-plane microbuckling in this unidirectional material is modelled as a bridged compressive mode I crack. A large-scale bridging model with an inferred tip toughness and a constant bridging stress is successful in predicting the propagation stress and overall kink-band widths. For T800/924C carbon/epoxy laminates the measured tip toughness is $G_C = 17.3\,\text{kJ m}^{-2}$ and the measured bridging stress is of the order of 100–133 MPa.

Finite element calculations have been used to predict this initiation behaviour and the early stages of growth of a microbuckle from a crack. The calculations predict the initial growth of two microbuckles from a sharp notch, in good agreement with experimental observations. R-curves (showing the dependence of the applied stress intensity factor on the microbuckle length) have been derived. The influence of matrix shear yield strain on the R-curve response is significant; the effect of strain-hardening exponent is relatively minor. The predicted microbuckle initiation load is found to be in good agreement with measured experimental data; the accuracy of the subsequent R-curve would be improved by a better constitutive model of the matrix at large strains.

ACKNOWLEDGEMENTS

Special thanks are due to Dr P. T. Curtis of the Defence Research Agency, Farnborough and Dr Yapa D. S. Rajapakse (Office of Naval Research, USA, grant number 0014-91-J-1916) for supporting this research. The PhD sponsorship offered to one of the authors (S. S.) from the Nanyang Technological University of Singapore (NTU), School of Mechanical and Production Engineering, is gratefully acknowledged. The technical assistance of Messrs R. Brand, R. Denston, S. Marshall, B. Butler, D. Miller and A. Heaver is appreciated.

REFERENCES

1 Awerbuch, J. and Madhukar, M.S. Notched strength in composite laminates: predictions and experiments—a review. *J. Reinforced Plastic Compos.* 1985, **4**, 3

2 Soutis, C., Curtis, P.T. and Fleck, N.A. Compressive failure of notched carbon fibre composites. *Proc. R. Soc. Lond. A* 1993, **440**, 241

3 Sutcliffe, M.P.F. and Fleck, N.A. Microbuckle propagation in carbon fibre–epoxy composites. *Acta Metall. Mater.* 1994, **42**, 2219

4 Sutcliffe, M.P.F. and Fleck, N.A. Compressive failure of notched carbon fibre–epoxy laminates. In 'Proc. European Conference on Composites Testing and Standards', Amsterdam, 1992, EACM, pp. 123–131

5 Sutcliffe, M.P.F. and Fleck, N.A. Effect of geometry on composites failure of notched composites. *Int. J. Fract.* 1993, **59**, 115
6 Peterson, R.E. 'Stress Concentration Factors', John Wiley, New York, 1974
7 Nuismer, R.J. and Labor, J.D. Application of the average stress failure criterion. Part II. Compression. *J. Compos. Mater.* 1979, **13**, 49
8 Rhodes, M.D., Mikulas, M.M. and McGowan, P.E. Effects of orthotropy and width on the compression strength of graphite/epoxy panels with holes. *AIAA J.* 1984, **22**, 1283
9 Whitney, J.M. and Nuismer, R.J. Stress fracture criteria for laminated composites containing stress concentrations. *J. Compos. Mater.* 1974, **8**, 253
10 Soutis, C., Fleck, N.A. and Smith, P.A. Failure prediction technique for compression loaded carbon fibre–epoxy laminate with an open hole. *J. Compos. Mater.* 1991, **25**, 1476
11 Argon, A.S. Fracture of composite. In 'Treatise of Materials Science and Technology', Vol. 1, Academic Press, New York, 1972
12 Budiansky, B. Micromechanics. *Computers & Struct.* 1983, **16**, 3
13 Budiansky, B. and Fleck, N.A. Compressive failure of fiber composites. *J. Mech. Phys. Solids* 1993, **41**, 183
14 Fleck, N.A., Deng, L. and Budiansky, B. Prediction of kink widths in fiber composites. *J. Appl. Mech.* 1995, **62**, 329
15 Slaughter, W.S., Fleck, N.A. and Budiansky, B. Compressive failure of fiber composites; the roles of multi-axial loading and creep. *J. Engng Mater. Technol.* 1993, **115**, 308
16 Moran, P.M., Liu, X.H. and Shih, C.F. Kink band formation and band broadening in unidirectional fiber composites under compression loading. *Acta Metall. Mater.* 1995, **43**, 2943
17 Fleck, N.A. and Budiansky, B. Compressive failure of fiber composites due to microbuckling. In 'Inelastic Deformation of Composite Materials' (Ed. G. J. Dvorak), Springer-Verlag, New York, 1991, pp. 235–274
18 Lagoudas, D.C. and Saleh, A.M. Compressive failure due to kinking of fibrous composites. *J. Compos. Mater.* 1993, **27**, 83
19 Wu, X.R. and Carlsson, A.J. 'Weight Functions and Stress Intensity Factor Solutions', Pergamon Press, Oxford, 1991
20 Sivashanker, S., Fleck, N.A. and Sutcliffe, M.P.F. Microbuckle propagation in a unidirectional carbon fibre–epoxy matrix composite, submitted to *Acta Metall. Mater.*
21 Paris, P.C. and Sih, G.C. Stress analysis of cracks. In 'Fracture Toughness Applications', ASTM STP 381, 1969, pp. 30–83
22 Soutis, C. and Fleck, N.A. Static compression failure of carbon fibre T800/924C composite plane with single hole. *J. Compos. Mater.* 1990, **24**, 536
23 Jelf, P.M. and Fleck, N.A. The failure of composite tubes due to combined compression and torsion. *J. Mater. Sci.* 1994, **29**, 3080
24 Sutcliffe, M.P.F., Fleck, N.A. and Xin, X.J. Prediction of compressive toughness for fibre composites, submitted to *Proc. R. Soc. Lond.*
25 ABAQUS manual, Version 5.3, Hibbitt, Karlsson & Sorensen, Inc., Providence, RI, 1994